



Fe-containing CeVO_4 films as Li intercalation transparent counter-electrodes

F. Artuso ^{a,*}, G. Picardi ^a, F. Bonino ^a, F. Decker ^a, S. Bencic ^b,
A. Surca Vuk ^b, U. Opara Krasovec ^b, B. Orel ^b

^a Chemistry Department and 'Istituto Nazionale di Fisica della Materia', University of Rome 'La Sapienza', I-00185 Rome, Italy

^b National Chemistry Institute, Hajdrihova 19, SI-1001 Ljubljana, Slovenia

Received 21 August 2000; received in revised form 10 November 2000

Abstract

Iron containing CeVO_4 films were prepared using the sol–gel method. The crystalline structure of powders and films with Fe/Ce/V ratios of 0.1:1:1, 0.3:1:1 and 0.5:1:1 were investigated by X-ray diffraction (XRD) and infrared (IR) spectroscopy. XRD revealed the predominance of a CeVO_4 -W (wakefieldite) crystalline phase with a small amount of monoclinic CeVO_4 , CeO_2 and Fe_2O_3 . Ex situ IR absorbance spectra of charged and discharged films show the changes in intensity of the V–O stretching mode at 770 cm^{-1} .

Cyclic voltammetry showed that Li^+ intercalation occurs in three steps with total capacities of 22 mC cm^{-2} (Fe/Ce = 0.1), 32 mC cm^{-2} (Fe/Ce = 0.3) and 37 mC cm^{-2} (Fe/Ce = 0.5). The increase in the overall charge capacity with increasing Fe content is accompanied by a loss of capacity with cycling. The lithium diffusion coefficient, calculated by the galvanostatic intermittent titration method (GITT), the potentiostatic intermittent titration method (PITT) and electrochemical impedance spectroscopy (EIS), ranges from 10^{-12} to $10^{-14}\text{ cm}^2\text{ s}^{-1}$. UV–vis in situ transmittance spectra showed that these films are highly transparent with a photopic transmittance $T_{\text{vis}} \sim 0.85$ for intercalated and deintercalated states. This suggests that Fe/Ce/V oxide films are good candidates for optically passive counter-electrodes in electrochromic (EC) devices. © 2001 Elsevier Science Ltd. All rights reserved.

Keywords: Fe-containing orthovanadates; Electrochromic film; Counter-electrodes

1. Introduction

There is a growing interest in the development of materials for electrochromic (EC) variable transmission glass devices. WO_3 is one of the most extensively investigated EC material giving the best EC performance due to its high charge capacity and long-term cyclability [1]. Less work has been devoted to the development of the appropriate counter-electrodes although many transition metal oxides have been proposed to work in

tandem with WO_3 in EC devices [2]. However, only those materials with a photopic transmittance above 70% in the intercalated state, a charge capacity comparable to WO_3 coupled to a high stability and reversibility with long-term cycling can be considered as promising optically passive counter-electrodes [3]. Among the various films studied to date, the rare-earth orthovanadates matched the desired properties for transparent counter-electrodes [4–9]. Studies by Picardi et al. [9] on Ce/V-oxides reveal that these oxides combine the properties of the parent oxides (V_2O_5 and CeO_2), i.e. the high ion-storage capacity of V_2O_5 and the optical passiveness of CeO_2 . Crystalline CeVO_4 films made using sol–gel synthesis and dip-coating

* Corresponding author.

E-mail address: artuso@uniroma1.it (F. Artuso).

deposition have the structure of the naturally occurring Wakefieldite. Stoichiometric Ce/V-oxide (CeVO_4) crystallises in a zircon-type structure consisting of VO_4 tetrahedra sharing edges with CeO_8 dodecahedra. The structure is rich in open space having channels running along the *c*-axis with a diameter suitable for the accommodation of Li^+ ions. The EC behaviour of CeVO_4 is close to that desired for optically passive counter-electrodes, the photopic transmittance T_{vis} being 0.900 in the charged and 0.902 in the discharged state, while the ion-storage capacity exceeds 20 mC cm^{-2} [7,8]. These results justify further development of Ce/V-oxide electrodes by modifying their structure by incorporating foreign ions into the CeVO_4 host.

We prepared ternary Fe/Ce/V-oxide films with molar ratios 0.1:1:1, 0.3:1:1 and 0.5:1:1. The reason for choosing iron as a structural modifier is that Fe and V form various Fe/V-oxides (i.e. FeVO_4 and $\text{Fe}_2\text{V}_4\text{O}_{13}$) which are recognised as promising intercalation compounds [4–6]. For example, FeVO_4 and $\text{Fe}_2\text{V}_4\text{O}_{13}$ films have charge capacities $> 20 \text{ mC cm}^{-2}$, small photopic coloration changes between the charged and discharged states (the difference in transmittance between the bleached and coloured state for FeVO_4 is 0.039 and for $\text{Fe}_2\text{V}_4\text{O}_{13}$ is 0.069) and a high electrochemical cycling stability [4–6]. Moreover, Fe^{3+} ions have the ability to be reduced during charging, which should increase the charging capacity. We expect that the addition of a small amount of Fe^{3+} will not significantly reduce the high transmittance of CeVO_4 . Accordingly, we performed extensive electrochemical and EC studies of Fe/V/Ce-oxide films to show whether they could be used as counter-electrodes in EC devices. Mainly, we want to assess how Fe^{3+} in the ternary oxide affects the structure of the films and, furthermore, how the modified structure changes their EC and electrochemical properties.

2. Experimental

All films were prepared by dip-coating deposition onto SnO_2/F glass substrates (K-glass, Pilkington plc.) using a simple dipping unit with a pulling speed of 10 cm min^{-1} . Vanadium-oxoisopropoxide (Fluka) and $\text{Fe}(\text{NO}_3)_3 \cdot 9\text{H}_2\text{O}$ were added to Ceria sols made by inorganic precursor $\text{CeCl}_3 \cdot 7\text{H}_2\text{O}$ (Fluka) mixed with citric acid in the proportion of 1:2 and dissolved in ethanol. Atomic ratios in the solutions were $\text{Fe/Ce/V} = 0.1:1:1$, $0.3:1:1$ and $0.5:1:1$. Following the deposition, the films were heated at 400°C for 60 min. Films thickness was measured with an Alpha step 200 profilometer and was about 100 nm. X-ray diffraction (XRD) measurements were carried out on powders obtained from the corresponding gels after thermal treatment at 400 and 500°C for 3 h. These measure-

ments were done using a Philips PW1710 (automated) X-ray diffractometer.

Ex situ absorbance IR measurements of films were carried out using a Perkin–Elmer System 2000 Spectrometer. The samples were prepared on double-side polished silicon wafers with $\rho = 200 \Omega \text{ cm}$. The electrical contacts on Si were made with an In–Ga alloy. The spectra have been recorded after galvanostatic charging and Li^+ discharging cycles.

Electrochemical measurements were performed in an argon filled dry box or in cells hermetically sealed under Ar atmosphere using an EG&G PAR 273 Potentiostat/Galvanostat. A Solartron Mod. 1255B Frequency Response Analyzer coupled with a potentiostat was used to measure the complex electrode impedance, taking an AC modulation amplitude of 10 mV in the frequency range from 100 KHz to 1 mHz. The electrochemical cell consisted of the working electrode, counter and reference electrodes of Li metal foils, dipped in 1 M $\text{LiClO}_4/\text{Propylene Carbonate}$ water free (Fluka) solution.

A HP 8452A diode-array spectrophotometer was used for transmittance measurements in the UV–vis region, taking a spectroelectrochemical cell filled with electrolyte as the background spectrum.

3. Results and discussion

3.1. X-ray structural analysis

The X-ray structural analysis was carried out on powders obtained from the corresponding gels after thermal treatment. The peaks attribution used for powders can be assumed to be valid for the films, although differences in the crystallisation rate between films and powders are possible. The XRD spectra of powders reveal that crystallisation occurs at 400°C while powders annealed at 300, 200 and 100°C are amorphous. The amount of iron in Fe/V/Ce-oxide powders influences their structure. As it is shown in Fig. 1, powders containing the smallest amount of iron ($\text{Fe/V/Ce} = 0.1:1:1$) show a predominance of the $\text{CeVO}_4\text{-W}$ (wakefieldite) phase (JCPDS 12-07571) with well defined grains ($\sim 30 \text{ nm}$) and a metastable monoclinic $\text{CeVO}_4\text{-Huttonite}$ (JCPDS 23-0150) phase. The diffraction peaks of the latter phase become less intense at a molar ratio of $\text{Fe/Ce/V} = 0.3:1:1$ and unobservable at $\text{Fe/Ce/V} = 0.5:1:1$ or when the temperature of heat treatment is raised to 500°C . Powders annealed at 400°C , irrespective of the amount of added iron, show admixed Fe_2O_3 (JCPDS 33-0664) and CeO_2 (JCPDS 43-1002) phases. It is significant that the former phase is in a smaller concentration than the CeO_2 phase, which becomes the secondary phase in the ternary oxide powders annealed at 500°C . This suggests that the presence of an amorphous iron-oxide phase is a characteristic feature of

Fe/Ce/V-oxide powders prepared at 400 and at 500°C, the main constituents being $\text{CeVO}_4\text{-W}$ and CeO_2 grains. In this respect, Fe/Ce/V-oxide films exhibit structural properties similar to that of $\text{CeO}_2/\text{TiO}_2$ films [10] where the nano-grains of CeO_2 are incorporated in the amorphous TiO_2 phase. The peak width of the main diffraction lines of the $\text{CeVO}_4\text{-W}$ phase, occurring at $2\theta = 47.9^\circ$, 32.4° and 24.0° , increases with an increasing iron concentration in powders heated at 400°C. The estimated grain size decreases from 30 to 20 nm with increasing Fe/Ce/V-oxide ratios. A similar decrease is noted for powders prepared at 500°C. A higher amount of iron leads to an increase in the amount of the CeO_2 phase. No Fe-oxide phase is found in XRD spectra of powders heated at 500°C, which supports the idea of the presence of an amorphous Fe-oxide phase serving as the host for the $\text{CeVO}_4\text{-W}$ and CeO_2 grains. Further evidence for this is the lack of the FeVO_4 phase expected in crystalline Fe/Ce/V-oxide powders. Because the structure of powders prepared at 400°C shows a strong dependence on the content of iron we focused our studies on this type of film to reveal how the crystallinity is reflected in their IR spectra and electrochemical properties.

3.2. IR spectra of films

IR and Raman spectra of crystalline CeVO_4 powders and films have been studied previously [7–9] and details concerning the vibrational band assignment have been reported elsewhere [11]. Because of a high symmetry of the $\text{CeVO}_4\text{-W}$ crystalline unit cell and of the presence of VO_4 tetrahedra, which are separated one from another by the bulky CeO_8 polyhedra, the IR spectrum consists of a single band centred at 770 cm^{-1} . This band is ascribed to the crystalline unit cell asymmetric stretching mode of VO_4 groups (E_u symmetry). An additional non-degenerated mode of the unit cell having A_u symmetry appears as a shoulder at 850 cm^{-1} while the deformational mode is assigned at 444 cm^{-1} . In terms of molecular group (VO_4^{3-} ion) modes, the crystalline E_u and A_u modes at 770 and 850 cm^{-1} belong to the split triply degenerate asymmetric stretching mode ν_3 (F_2) appearing in the spectra of VO_4^{3-} ions in solutions at 790 cm^{-1} [12], while the 440 cm^{-1} band of the crystalline unit cell corresponds to the triply degenerate ν_4 deformational mode of isolated VO_4^{3-} ions at 340 cm^{-1} [12]. The totally symmetric (ν_1) mode of the CeVO_4 unit cell is found only in the Raman spectra at 824 cm^{-1} [12] and will not be discussed further.

We expect that the changes of the grain size noted in the XRD spectra of Fe/Ce/V-oxide powders containing different amounts of iron will be reflected in the broadness of the 770 cm^{-1} band and in the appearance of new modes (Fig. 2A). In addition, the A_u IR active symmetric mode is expected to change in intensity because of the relaxation of the selection rules of the crystalline unit cell symmetry, allowing the activation of the internal modes of VO_4 units in the crystalline cell.

IR spectra of Fe/Ce/V (0.3:1:1) and (0.5:1:1) films annealed at 400°C reveal that besides the central band at 770 cm^{-1} two additional broad shoulder bands at 870 and 728 cm^{-1} appear indicating a less defined crystalline $\text{CeVO}_4\text{-W}$ phase. Conversely, IR spectra of Fe/Ce/V (0.1:1:1)-oxide films reveal only a sharp singlet at 770 cm^{-1} with a weak shoulder band at 870 cm^{-1} and an unsplit deformational mode at 444 cm^{-1} , which are characteristic for the $\text{CeVO}_4\text{-W}$ phase. This means that the presence of iron in the films retards the formation of the $\text{CeVO}_4\text{-W}$ phase, in good agreement with the XRD results. When the temperature of heat-treatment is raised to 500°C the IR spectra of all three types of Fe/Ce/V-oxide films become similar having the characteristics of the $\text{CeVO}_4\text{-W}$ phase with the exception that in the spectrum of Fe/Ce/V (0.5:1:1)-oxide the shoulder band (A_u) at $830\text{--}890\text{ cm}^{-1}$ increases in intensity (Fig. 2A). This indicates the disturbing effect of iron on the $\text{CeVO}_4\text{-W}$ grains.

Ex situ IR absorbance spectra of a charged/discharged Fe/Ce/V (0.3:1:1)-oxide film prepared at 400°C are presented in Fig. 2B. The film deposited on a silicon

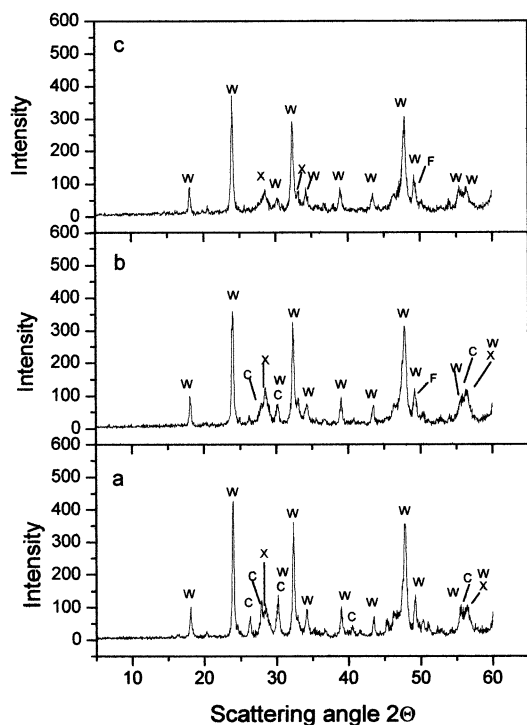


Fig. 1. XRD spectra of Fe_xCeVO_4 powders annealed at 400°C for 3 h: (a) $x = 0.1$; (b) $x = 0.3$; (c) $x = 0.5$. $\text{CeVO}_4\text{-W}$ -akefieldite (W); $\text{CeVO}_4\text{-Huttonite}$ (C); CeO_2 (X); Fe_2O_3 (F).

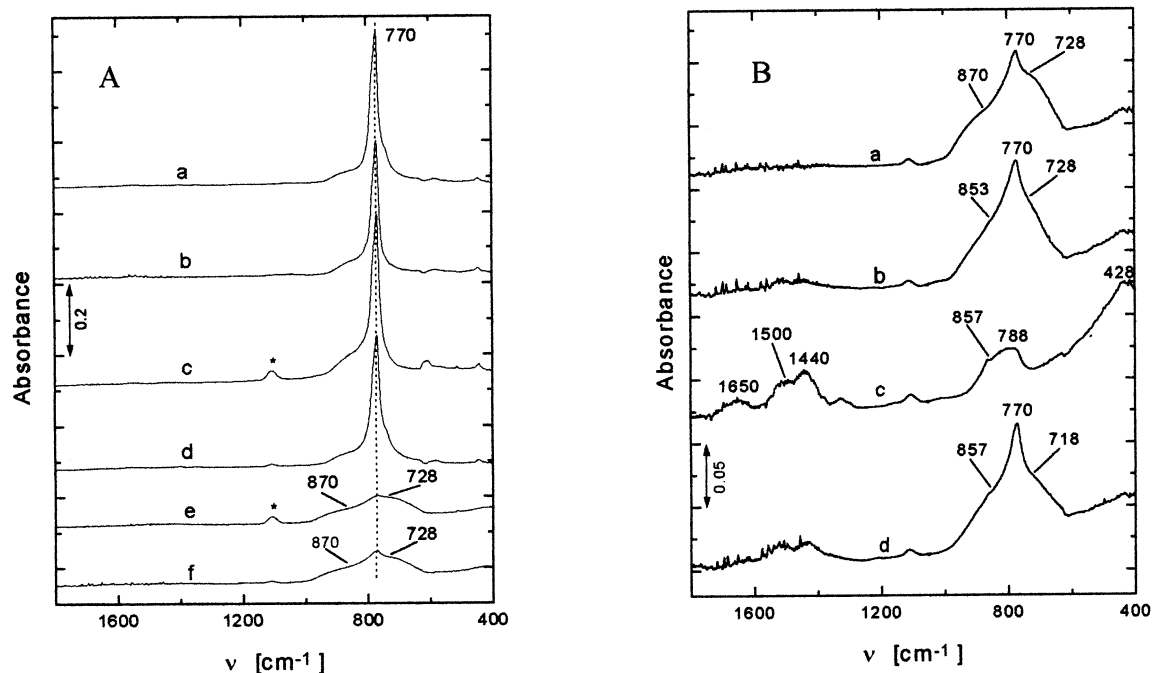


Fig. 2. (A) Absorbance IR spectra of Fe/Ce/V-oxide films deposited on silicon wafers: (a) $\text{Fe}_{0.1}\text{CeVO}_4$, 500°C; (b) $\text{Fe}_{0.3}\text{CeVO}_4$, 500°C; (c) $\text{Fe}_{0.5}\text{CeVO}_4$, 500°C; (d) $\text{Fe}_{0.1}\text{CeVO}_4$, 400°C; (e) $\text{Fe}_{0.3}\text{CeVO}_4$, 400°C; and (f) $\text{Fe}_{0.5}\text{CeVO}_4$, 400°C. All films were heated for 1 h. The peaks labelled with * are due to substrate impurities. (B) Ex situ IR absorbance spectra of $\text{Fe}_{0.3}\text{CeVO}_4$ film (400°C, 1 h) charged galvanostatically using a current of $27.8 \mu\text{A cm}^{-2}$: (a) as-deposited state, (b) charged down to 1.7 V vs. Li, (c) charged down to 0.8 V vs. Li and (d) discharged up to 5.3 V vs. Li. The electrolyte used was 1 M LiClO_4/PC .

wafer was galvanostatically charged with a current density of $27.8 \mu\text{A cm}^{-2}$ down to the potential limits of 1.7 and 0.8 V. These potentials are more negative when compared to the potentials at which the reactions proceed for the same films deposited on SnO_2/F glass (Section 3.3). The reason for the high overpotential of the electrochemical processes on silicon wafers is the higher electrical resistivity ($\sim 200 \Omega \text{ cm}$) compared with SnO_2/F glass. However, the shape of the galvanostatic charging of Fe/Ce/V (0.3:1:1)-oxide film deposited on either silicon or SnO_2/F resembles each other, showing that the ex situ IR spectra of the film charged to 1.7 and 0.8 V can be correlated to the electrochemical processes A' and B' in the cyclic voltammetric responses shown in Fig. 3 (Section 3.3).

Galvanostatic charging of the Fe/Ce/V (0.3:1:1)-oxide film down to 1.7 V (A' peak) results in a small increase in the intensity of the 770 cm^{-1} band, which is attributed to the asymmetric stretching of VO_4 groups, while the shoulder bands at 870 and 728 cm^{-1} become less distinct (Fig. 2B–b). The changes in the IR spectra are more pronounced after charging down to 0.8 V (B' peak) (Fig. 2B–c). The intensity of the central band at 770 cm^{-1} decreases significantly and a broad absorption appears below 600 cm^{-1} . On the basis of our previous studies [5,6], the latter can be attributed to the

$\text{Li}^+ - \text{O}$ modes of Li^+ ions vibrating against the oxygen host overlapping with the $\text{V}^{4+} - \text{O}$ skeletal modes also appearing in IR spectra of charged V_2O_5 , FeVO_4 and $\text{Fe}_2\text{V}_4\text{O}_{13}$ [4–6]. After discharging at 5.3 V the IR spectrum (Fig. 2B–d) is almost identical to the initial spectrum (Fig. 2B–a), showing that the intercalation of Li^+ ions is reversible during the first two electrochemical steps (A', B'). The observed changes in intensity of the 770 cm^{-1} band in Fig. 2B match closely those of Li_xCeVO_4 films charged/discharged in the same domain of the intercalation coefficient $0 < x < 1$ [7–9] and could be correlated to the variations in the electrical conductivity of films charged to different extents [13].

3.3. Cyclic voltammetry

The cyclic voltammeteries (CVs) of the films obtained from starting solutions with Fe/Ce/V ratios 0.1:1:1, 0.3:1:1 and 0.5:1:1 are reported in Fig. 3. The scan rate was 5 mV s^{-1} and the potential window was between 1.0 and 4.3 V vs. Li (CVs at faster scan rates were recorded too but are not reported here).

The CVs relative to the film with lower Fe content (Fe/Ce/V 0.1:1:1 films) are very similar to those of stoichiometric CeVO_4 CVs [9]: as for CeVO_4 films, two distinct electrochemically active regions appear, one at

potentials between 4.3 and 2.6 V and another between 1.8 and 1.0 V. The peak labelling previously used for CeVO_4 CVs can be adopted here again because all the three processes denoted by letters A/A', B/B' and C/C' (' is used for cathodic peaks) are typical for lithium intercalation in crystalline CeVO_4 -W. The process A' is a convolution of two peaks that can be easily resolved at very low scan rate into its two components at potentials 2.8 and 3.2 V, marking the initial lithium intercalation into two different sites in the host structure. This process is linked to the vanadium reduction of a portion of V atoms, belonging to VO_4^{3-} units, to the 4+ oxidation state. Complete reduction to V^{3+} states takes place at potentials lower than 1.8 V (peaks B' and C').

A small cathodic peak (D'), absent in CeVO_4 CVs, appears at 1.5 V, coupled with a pronounced shoulder

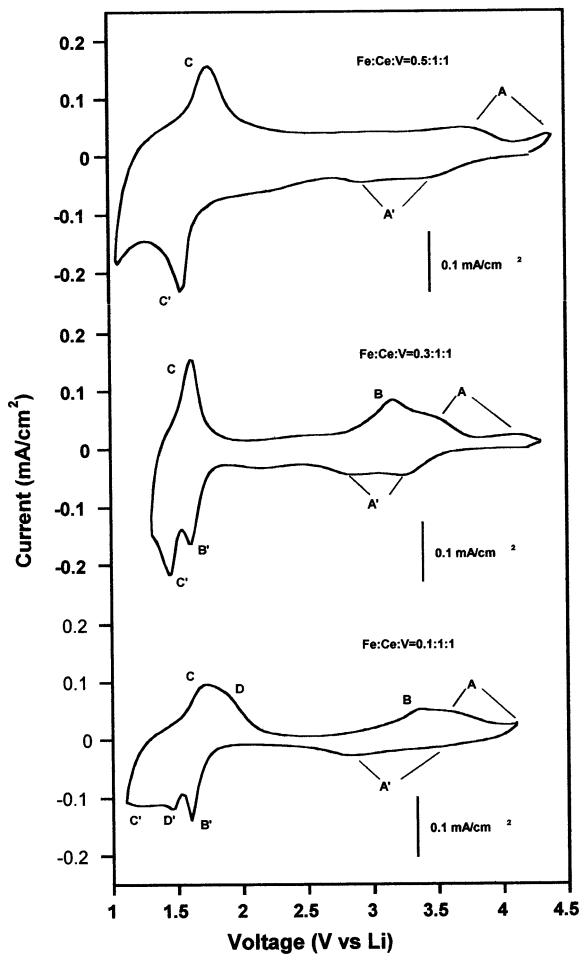


Fig. 3. CVs responses of Fe/Ce/V = 0.1:1:1, 0.3:1:1 and 0.5:1:1 films in 1 M LiClO_4/PC anhydrous electrolyte, with a Li reference electrode. Potential window: 1.0–4.3 V vs. Li. Scan rate: 5 mV s^{-1} .

(D) on the right of peak C, at about 2.0 V. For a typical cycle at 10 mV s^{-1} , the intercalated/deintercalated charges are $-22.4/21.8 \text{ mC cm}^{-2}$.

The intermediate potential zone (1.8–2.6 V) bears a considerable amount of charge for the films with Fe/Ce/V = 0.3:1:1, whereas in CeVO_4 CVs the same potential region lacked any current response. Lithium intercalation at these potential values may be promoted by the presence of reducible Fe^{3+} cations in the amorphous phase. The activation of a new potential region for the intercalation process increases the overall lithium charge capacity: the calculated cathodic and anodic charges for a cycle at 10 mV s^{-1} scan rate are $-32.0/31.0 \text{ mC cm}^{-2}$.

Even higher values, $-36.5/32.6 \text{ mC cm}^{-2}$, are obtained from the initial cycles of films with Fe/Ce = 0.5. The CVs shape still resembles that of a stoichiometric CeVO_4 film, but some details are lost due to the current plateau stretching from 3.5 down to 1.0 V; this current is probably associated to the reduction of Fe^{3+} atoms overtaking the further reduction of vanadium to V^{3+} states. There might also be the contribution of the cerium electrochemical activity, indeed those potential values are typical for lithium intercalation–deintercalation inside CeO_2 amorphous films [14,15].

The films with the highest iron content are not stable towards lithium intercalation. In fact after 20 cycles of Li intercalation–deintercalation the charge capacity decreased to $-5.6/4.3 \text{ mC cm}^{-2}$ and the CV shows no signs of vanadium electrochemical activity. Peaks C/C' are the first to fade away, then some structural change (observed during galvanostatic cycling) can undergo inside the fully intercalated film, probably leading to a more stable amorphous phase saturated with lithium, thus limiting further intercalation.

No such effect has been observed for the other films with a Fe/Ce ratio less than 0.5. After 300 cycles the intercalated–deintercalated charges are $-18.1/17.9 \text{ mC cm}^{-2}$ for Fe/Ce = 0.1 films and $-22.1/21.6 \text{ mC cm}^{-2}$ for Fe/Ce = 0.3 films. In this case, the charge capacity losses are probably due to a small fraction of lithium irreversibly intercalated inside the film that can no longer be extracted and normally cycled in the potential range used.

3.4. Complex impedance spectra

AC electrochemical complex impedance spectra have been taken in the frequency range from 100 KHz to 1 mHz for films in the pristine state and at the potential of 1.5 V vs. Li. Before performing impedance experiments all samples were submitted to some activation charge/discharge voltammetric cycles.

In Fig. 4 the Nyquist plots of a Fe/Ce/V 0.5:1:1 sample in the pristine state and at the cathodic potential of 1.5 V (fully intercalated) are reported. The film

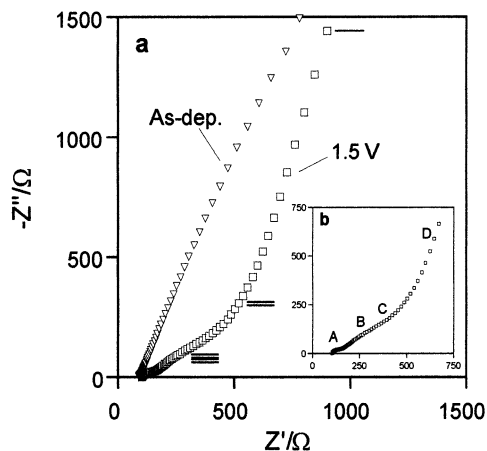


Fig. 4. (a) Nyquist plots of Fe/Ce/V 0.5:1:1 films, as deposited and at the potential of 1.5 V; (b) magnification of the spectrum at 1.5 V (inserted charge = 18 mC cm⁻²). Symbols, —, =, ≡, indicate the frequencies of 10 mHz, 100 mHz, 1 Hz, respectively. All frequencies for the spectrum of as-deposited film are over 2 Hz.

as deposited shows a capacitive impedance response, while the interpretation of intercalated sample data are more complex. The high frequency semicircle (zone A in Fig. 4b) is probably due to a passivation layer covering the electrode surface while the second semicircle partially visible in the zone B can be attributed to a charge transfer process. In zone C the spectrum displays a Warburg impedance, associated with the Li⁺ seminfinitesimal diffusion inside the oxide film. At very low frequencies (zone D) the sample shows a capacitive behaviour, due to the finite path of the diffusion process in the thin film.

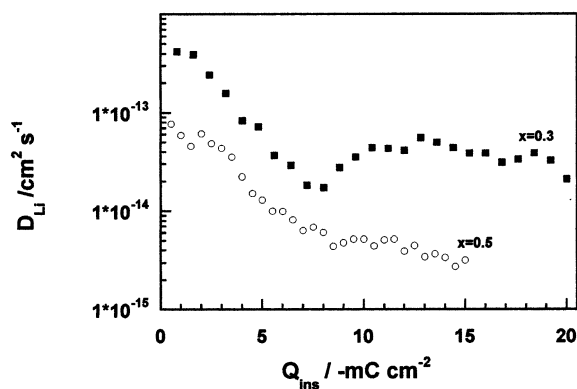


Fig. 5. Lithium diffusion coefficients versus intercalated charge for Fe/Ce/V = 0.3:1:1 and 0.5:1:1 films, from GITT measurements during Li intercalation. Constant current pulses of 0.1 mA cm⁻².

The low frequency part of the spectrum was then used to calculate the lithium diffusion coefficient D_{Li} according to the following formula [16]:

$$D_{Li} = \frac{Z'' 2\pi\nu l^2}{3R_L}$$

where Z'' is the imaginary part of the impedance at a frequency ν , R_L the limiting resistance and l the film thickness. The calculated value of the diffusion coefficient D_{Li} is 8.5×10^{-13} cm² s⁻¹ for Fe/Ce = 0.5 films. The calculation of D_{Li} , in the same conditions, was made for Fe/Ce = 0.1 films and it was found to be 1.2×10^{-12} cm² s⁻¹. These values are in good agreement with the results coming out from potentiostatic intermittent titration technique (PITT) measurements.

3.5. PITT and GITT measurements

The diffusion coefficients calculated by EIS were compared to the ones obtained by PITT. The PITT measurements were carried out around the same potential peak at 1.5 V and on the same films, just before the EIS experiment. To calculate the diffusion coefficient D_{Li} of Li inside the film, the plot of $I^{1/2}$ vs. $\log t$ was analysed. According to such theoretical treatment, the Cottrell region is represented by a plateau, with a characteristic $I^{1/2}$ constant value. D_{Li} can be calculated by the following equation [17]:

$$I^{1/2} = \frac{D_{Li}^{1/2} \Delta Q}{l \pi^{1/2}}$$

where $I^{1/2}$ is the value obtained in the Cottrell domain, ΔQ the amount of charge injected into the electrode during the potential step and l the thickness of the film. The average diffusion coefficients calculated for Fe/Ce = 0.5 and Fe/Ce = 0.1 films were found to be 8.6×10^{-13} and 2.5×10^{-12} cm² s⁻¹, respectively.

The trend of D_{Li} throughout the whole intercalation process was followed by galvanostatic intermittent titration technique (GITT) [18]. 100 μ A cm⁻² current density and pulses of 5 s were used for the stepwise intercalation. Between one pulse and the following one 30 min were left for the relaxation (lithium diffusion) to take place inside the film. The potential values before the pulse, at the end of the pulse and after the relaxation, respectively, E_i , E_p , E_r , have been recorded in order to calculate the lithium diffusion coefficients using the following formula:

$$D_{Li} = \frac{4l^2}{\pi\tau} \left(\frac{E_i - E_r}{E_r - E_i} \right)^2$$

where l is the film thickness and τ the pulse duration, E_i the difference between the initial potential E_i and the IR drop.

Fig. 5 reports the diffusion coefficients for the films with Fe/Ce/V = 0.3:1:1 and Fe/Ce/V = 0.5:1:1. A faster

lithium diffusion is observed for the film with the lower Fe content (Fe/Ce = 0.3), for which two diffusional mechanisms seem to be involved. Initially D_{Li} decreases steadily from 4×10^{-13} to 1×10^{-14} $\text{cm}^2 \text{s}^{-1}$ and this may indicate that diffusion preferentially takes place through the defined channels of the crystalline phase ($\text{CeVO}_4\text{-W}$). Later on D_{Li} reaches a quite stable value around 3×10^{-14} $\text{cm}^2 \text{s}^{-1}$, typical of diffusion inside an amorphous phase. The values of the diffusion coefficients by GITT are much lower than the D_{Li} calculated by EIS and PITT, which may be more accurate for a specific electrode potential. Nevertheless, the results from GITT are valuable, because they give the overall trend of D_{Li} as a function of the intercalated charge.

3.6. In situ UV–vis spectroscopy

Stoichiometric CeVO_4 films are highly transparent in the visible range and display a minimal mixed cathodic/anodic EC effect [9]. Two different absorption mechanisms, namely band-gap widening and polaron absorption, are needed to explain this mixed optical behaviour. The UV–vis spectra of Fe/Ce/V films, taken in situ during lithium intercalation–deintercalation, follow closely the $\text{CeVO}_4\text{-W}$ transmittance spectra (Fig. 6).

In fact, there is a transmittance decrease (cathodic electrochromism) at wavelengths > 450 nm due to polaron absorption [19], while for $\lambda < 450$ nm a cathodic bleaching is observed with intercalation of Li. This spectral transmittance increase at low wavelength is attributed to band gap widening [19] and it is typical of V-containing oxides [6,8,19].

The optical data obtained by UV–vis measurements were elaborated in terms of photopic transmittance (T_{vis}) according to the following formula [6]:

$$T_{vis} = \frac{\int_{\lambda=350 \text{ nm}}^{820 \text{ nm}} T(\lambda)R(\lambda) d\lambda}{\int_{\lambda=350 \text{ nm}}^{820 \text{ nm}} R(\lambda) d\lambda}$$

where $T(\lambda)$ represents spectral transmittance of the sample and $R(\lambda)$ the eye spectral response. The T_{vis} of the films in the deintercalated (intercalated) states were found to be 87.4% (86.6%), 87.3% (85.9%), and 84.8% (79.9%) for Fe/Ce 0.1, Fe/Ce 0.3 and Fe/Ce 0.5 films, respectively.

The most remarkable consequence of the presence of Fe atoms in the films is a small lowering in the average transmittance for $\lambda > 400$ nm. Fe/Ce = 0.5 films are the less transparent samples due to the presence of Fe^{3+} absorbing species. Nevertheless our studies showed that optical passiveness in the thermal solar range (> 600 nm) are quite as good as that of CeVO_4 .

4. Conclusions

The electrochemical and optical properties of iron containing CeVO_4 films obtained by the sol–gel method were studied and compared. We showed that the presence of Fe allows higher ion-storage capacity (compared to CeVO_4) exceeding 30 mC cm^{-2} , although some drawbacks come from it.

XRD spectra of powders revealed that Fe^{3+} in the films affects the structure of the oxide: higher amount of iron in Fe/Ce/V-oxide leads to a decrease in grain size and to an increase in the quantity of the CeO_2 phase. This is confirmed by IR spectra: changes of grain size have been reflected in the broadness of the 770 cm^{-1} band and the appearance of new modes. This means that the presence of Fe retards the formation of the $\text{CeVO}_4\text{-W}$ phase and brings about more amorphous compounds.

Cyclic voltammetry and galvanostatic measurements showed that Fe leads to an increase in the overall lithium charge capacity but this is associated with higher loss of capacity with cycling (from 37 to 5 mC cm^{-2} after 20 cycles for Fe/Ce/V 0.5:1:1 films). Probably structural changes occur inside the fully intercalated film, leading to a more stable amorphous phase saturated with Li, thus limiting further intercalation. GITT, PITT and AC impedance spectroscopy showed that diffusion coefficients values D_{Li} decrease one order of magnitude when passing from Fe/Ce = 0.1, Fe/Ce = 0.3 and to Fe/Ce = 0.5 films. A good agreement on D_{Li} at the electrode potential of 1.5 V was found with PITT and EIS, giving values in the range of $10^{-12} \text{ cm}^2 \text{s}^{-1}$.

Finally Fe doped Ce/V-oxide films have less favourable optical properties due to the presence of Fe^{3+} absorbing species but our studies showed that optical passiveness in the spectral eye response range (350–820 nm) is not dramatically worse as regards that of

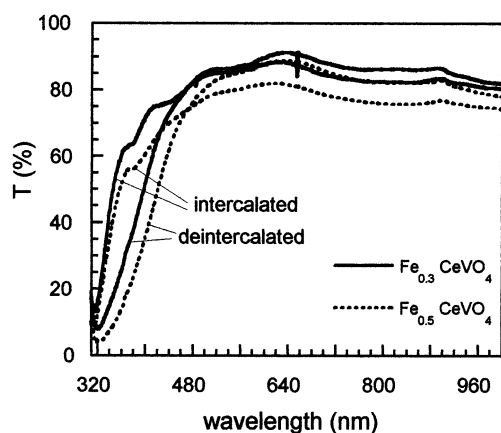


Fig. 6. Transmittance spectra taken in situ after Li insertion–deinsertion performed in 1 M LiClO_4/PC anhydrous electrolyte. Inserted charge: $\text{Fe}_{0.3}\text{CeVO}_4 = 11 \text{ mC cm}^{-2}$; $\text{Fe}_{0.5}\text{CeVO}_4 = 15 \text{ mC cm}^{-2}$.

CeVO₄, giving a photopic transmittance of about 0.85. These results suggest that Fe/Ce/V-oxide films are good candidates as optically passive counter-electrodes for EC devices.

References

- [1] C.G. Granqvist, *Handbook of Inorganic Electrochromic Materials*, Elsevier, Amsterdam, 1995.
- [2] M.A. Aegerter, *Sol-gel Chromogenic Materials and Devices, Structure and Bonding*, vol. 85, Springer, Berlin, 1996, pp. 149–194.
- [3] U. Opara Krasovec, A. Surca, B. Orel, EuroSun 2000, June 19–22, 2000, Copenhagen, Denmark (to be published in Proceedings).
- [4] S. Bencic, B. Orel, A. Surca, U. Lavrencic Stangar, *Solar Ener.* 68 (2000) 499.
- [5] A. Surca, B. Orel, G. Drazic, F. Decker, P. Colomban, submitted to *Sol-Gel Sci. Technol.*
- [6] A. Surca, B. Orel, U. Opara Krasovec, U. Lavrencic Stangar, G. Drazic, *J. Electrochem. Soc.*, 147 (2000), in press.
- [7] U. Opara-Krasovec, B. Orel, R. Reispeld, *Electrochem. Sol. State Lett.* 1 (1998) 104.
- [8] U. Opara Krasovec, B. Orel, A. Surca, N. Bukovec, R. Reispeld, *Solid State Ionics* 118 (1999) 195.
- [9] G. Picardi, F. Varsano, F. Decker, U. Opara-Krasovec, A. Surca, B. Orel, *Electrochim. Acta* 44 (1999) 3157.
- [10] D. Keomany, J.-P. Petit, D. Deroo, *Proc. SPIE* 2255 (1994) 363.
- [11] E.J. Baran, M.E. Escobar, L.L. Fourier, R.R. Filgueira, *Z. Anorg. Allg. Chem.* 472 (1981) 193.
- [12] A. Muller, E.J. Baran, P.J. Hendra, *Spectrochim. Acta* 25A (1969) 1654.
- [13] P. Colomban, J.-C. Badot, Frequency dependent conductivity, microwave dielectric relaxation and proton dynamics, in: P. Colomban (Ed.), *Proton Conductors, Chemistry of Solid State Materials*, vol. Vol. 2, Cambridge University Press, Cambridge, 1992, p. 391.
- [14] U. Lavrencic Stangar, B. Orel, I. Grabec, B. Ogorevc, K. Kalcher, *Sol. Ener. Mater. Sol. Cells* 31 (1993) 171.
- [15] D. Keomany, J.P. Petit, D. Deroo, *Sol. Ener. Mater. Sol. Cells* 36 (1995) 397.
- [16] C. Ho, I.D. Raistrick, R.A. Huggins, *J. Electrochem. Soc.* 127 (1980) 343.
- [17] M.D. Levi, E.A. Levi, D. Aurbach, *J. Electroanal. Chem.* 421 (1997) 89.
- [18] W. Weppner, R.A. Huggins, *J. Electrochem. Soc.* 124 (1977) 1569.
- [19] A. Talledo, C.G. Granqvist, *J. Appl. Phys.* 77 (1995) 4655.